BIFURCATING NEURONS IN THE ANTERIOR THALAMIC NUCLEI

Pei Y*,[1-3] Tasananukorn S (Yee T)*,[1-3] Wolff M,[4,5] Dalrymple-Alford JC.[1-3]

* Equal first authors

1. School of Psychology, Speech and Hearing, University of Canterbury, 20 Kirkwood Avenue, Christchurch 8041, New Zealand

2. New Zealand Brain Research Institute, 66 Stewart Street, Christchurch 8011, New Zealand

3. Brain Research New Zealand – Rangahau Roro Aotearoa

4. CNRS, INCIA, UMR 5287, Bordeaux, France

5. University of Bordeaux, INCIA, UMR5287, Bordeaux, France

Abstract

The anterior thalamic nuclei (ATN) form a nodal point within a hippocampal-cingulate-diencephalic memory system. ATN projections to different brain structures are conventionally viewed as distinct, but ATN neurons may send collaterals to multiple structures. The anteromedial subregion (AM) is the primary source of efferents to the medial prefrontal cortex (mPFC). Using a dual-retrograde neurotracer strategy, we discovered bifurcating AM neurons for tracers placed in the mPFC when paired with other regions. A semi-quantitative analysis found a high proportion of AM neurons (~36%) showed collateral projections when the mPFC was paired with dorsal subiculum (dSub); 20% were evident for mPFC paired with caudal retrosplenial cortex (cRSC); and 6% was found for mPFC and ventral hippocampal formation (vHF). About 10% of bifurcating AM neurons was also identified when the mPFC was not included, that is, for cRSC with dSub, and cRSC with vHF. Similar percentages of bifurcating neurons were also found within the anterior region of the adjacent nucleus reuniens (Re). The high frequency of bifurcating neurons suggests a new perspective for ATN function. These neurons would facilitate direct coordination among distal neural ensembles to support episodic memory and may explain why the ATN is a critical region for diencephalic amnesia.

Introduction

The anterior thalamic nuclei (ATN) constitute a strategic node in a hippocampal-cingulate diencephalic-memory network (Aggleton et al., 2016; Bubb et al., 2017; Nelson, 2021; Vann et al., 2009). The ATN have reciprocal connections with at least three distinct memory structures, namely the medial prefrontal cortex (mPFC), retrosplenial cortex (RSC) and subicular regions of the hippocampal formation (HF) (Bubb et al., 2017; Mathiasen et al., 2017). The importance of the ATN for memory is supported by extensive clinical and experimental evidence (Aggleton, 2008; Aggleton et al., 2016; Barnett et al., 2021; Carlesimo et al., 2011; Dalrymple-Alford et al., 2015; Harding et al., 2000; Kim et al., 2009; Kopelman, 2015; Liu et al., 2021; Maillard et al., 2021; Sweeney-Reed et al., 2021; Wolff et al., 2015). This evidence is consistent with the perspective that the ATN are a critical hub that actively coordinates information processing among telencephalic memory structures (Wolff and Vann, 2019).

The ATN's neural connections with different cortical and hippocampal regions are viewed as arising from predominantly separate neuronal populations that give rise to hierarchically organised functional subsystems (Aggleton et al., 2010; Jankowski et al., 2013; Mathiasen et al., 2020; Nelson, 2021; Shibata, 1993a, 1993b; van Groen et al., 1999; van Groen and Wyss, 1990; van Groen and Wyss, 1995). This conventional perspective emphasises functionally segregated, if not independent, ATN circuits with little if any direct integration across the ATN's terminal projection fields. Although segregated projections may be particularly relevant for cortico-thalamic projections, it is less clear if the reverse projections are equally distinct (Aggleton et al., 2010; Mathiasen et al., 2020; Nelson, 2021). The thalamo-cortical projections from different ATN subnuclei show some regional overlap in many of their terminal fields.

The overlap among terminal fields for ATN efferents is consistent with the proposal for an active role by the ATN in coordinating memory-related information (Wolff and Vann, 2019). This idea would, however, be strengthened by evidence that a subpopulation of ATN neurons send collateral projections to distinct terminal regions, such as the mPFC, RSC and / or HF. Sripanidkulchai and Wyss (1986), however, found little if any evidence that ATN axons collateralize, at least with respect to the rostral and caudal aspects of the agranular RSC in the rat. This negative finding does not rule out the possibility of other collateralizations especially among more distant terminal regions. One existing lead to support the prospect of bifurcating ATN neurons comes from a study that used a double neuroanatomical labelling technique for ATN projections to the different areas of the cingulate gyrus in rats (Horikawa et al., 1988). They reported that ATN neurons send collateral projections to anterior and posterior sub-areas within the anterior cingulate cortex (ACC; part of the dorsal mPFC) and within the RSC. More direct encouragement for the idea that ATN neurons send collaterals to influence different memory structures is that Horikawa et al. (1988) also found evidence that about 6% to 13% of the projection neurons from the anteromedial thalamic nucleus (AM) of the ATN send bifurcating axons to both the anterior ACC and the posterior RSC.

We, therefore, examined whether a subpopulation of ATN neurons send projections simultaneously to pairs of distantly-located neuronal structures associated with memory and related cognitive processes. Following the preliminary evidence from Horikawa et al. (1988), our primary interest was the AM subregion of the ATN. There is good reason to focus on this subregion as it is clearly the primary source of ATN projections to the mPFC, but it also has projections to both dorsal HF and ventral HF (vHF), and the RSC (Bubb et al., 2017; Shibata, 1993; van Groen and Wyss, 1995; van Groen et al., 1999). We used a double retrograde neurotracer technique to examine ATN projections to the mPFC paired with the dorsal

subiculum (dSub), mPFC paired with vHF, and mPFC paired with caudal RSC (cRSC). Additional comparisons came from paired retrograde neurotracers that did not include the mPFC, that is, the cRSC paired with the dSub, and the cRSC paired with vHF. A given pair of these terminal regions for ATN efferents each received one of two retrograde tracers, specifically Cholera Toxin Subunit B (CTB) conjugated to either Alexa Fluor® 488 or 594. These tracers overcome the relative imbalance of labelling that can be found, for example, with Fast Blue combined with Rhodamine microspheres as was used in the study by Horikawa et al. (1988). CTB tracers have been shown to be sensitive and reliable for neuroanatomical retrograde tracing in double-labelling studies, including work on the thalamic reuniens (Re), the anterior region of which is located immediately beneath the AM (Conte et al., 2009a, 2009b; Varela et al., 2014). We found a substantial number of bifurcating AM neurons in each of the five combinations of CTB infusion placements, especially when one retrograde neurotracer in the mPFC was paired with another placed in the dSub or cRSC.

Materials and Methods

Animals and housing conditions

We used 22 male Piebald Virol Glaxo cArc hooded rats, bred in the Animal Facility at the University of Canterbury and maintained in standard housing of three or four rats per opaque plastic cage (50 cm long x 30 cm wide x 23 cm high). The rats were 6-7 months at the time of surgery. Single housing was used for the 9-days of recovery following surgery, which enabled uptake of the retrograde tracers before euthanasia and histology. Food and water were available ad libitum. All procedures were approved by the University of Canterbury Animal Ethics Committee (#2018/26R).

Surgery and infusion of retrograde neurotracers

Two Cholera Toxin Subunit B (Recombinant) Alexa Fluor™ (AF CTB) neurotracers were used. These were AF CTB 488 conjugate and AF CTB 594 conjugate (Life technologies New Zealand Limited, Auckland, NZ). The tracers were used at 1% concentration (500ug in 50ul in neutral phosphate buffer), prepared by gentle rotation plus 1 sec centrifuge of the vial, in order to avoid denaturing that occurs with vortexing. Vials were stored upright at 4˚C for up to one week. We only used separate syringes for each tracer to prevent contamination. Each rat was injected with one tracer in one terminal region of the ATN and, in the same hemisphere, the second tracer in a second terminal region of the ATN (always the right hemisphere).

Our primary focus was to examine AM neurons projecting to the following distally-located terminal fields: (1) mPFC and dSub (n=4), (2) mPFC and vHF (n=4) and (3) mPFC and cRSC (n=3). The “mPFC and vHF” pairing has been used in previous work to identify bifurcating neurons in the Re (Hoover and Vertes, 2012; Varela et al., 2014), so this enabled a direct comparison between the AM and the rostral aspects of the Re. Given the lengthy rostro-caudal extent of the cingulate gyrus, we restricted our focus on the cRSC only, but across both areas 29b and 29c. For comparison, two additional pairings were included without the mPFC, namely (4) cRSC and dSub (n=1) and (5) cRSC and vHF (n=2). Infusions in the cRSC, however, was challenging because sometimes there was either minimal or even no sign of any CTB neurotracer. This led to the exclusion of some additional rats: mPFC and

cRSC, n=2; cRSC and dSub, n = 3; and cRSC and vHF, n=2. Also, one case with an intended pairing of mPFC with vHF (Case Y6) was excluded as it had vHF infusion that was posterior and too ventral, showing neurotracer in only the entorhinal cortex.

For infusions, rats were anaesthetized with 4% isoflurane and placed in a stereotaxic frame with atraumatic ear bars (Kopf, Tujunga, CA, USA) with the dorsal surface of the skull held in a flat position. Anaesthesia was maintained with 2% isoflurane. We infused the neurotracers via a 10 µl NanoFil syringe (blunt tip, 33-gauge needle; World Precision Instruments, Sarasota, FL, USA) at a rate of 0.05 µl / minute using a micro-infusion pump (Stoelting, Wood Dale, IL, USA). The syringe needle was lowered slowly to each coordinate and left in situ for 5 min post-infusion at each site for diffusion of the tracer. Within each target pairing, the two CTB tracers were counterbalanced across the two terminal regions. To ensure maximal coverage within each terminal region and increase uptake by ATN terminals, two x 0.6 µl (of the same tracer) infusions were made in each structure (i.e. 1.2 µl for each structure). So, an upper and a lower site was used for the mPFC; and one anterior and one posterior site was used for each of the dSub, vHF, and cRSC. For mPFC, the coordinates were: upper site (cingulate cortex, area 32D), AP + 3.0 mm from Bregma, LAT – 0.6 mm, DV – 2.2 mm; and - 3.5 mm, lower site (cingulate cortex, area 32V). For dSub: anterior, AP – 6.6 mm from bregma, LAT - 3.6 mm, DV - 3.1 mm; posterior, AP – 7.1 mm from bregma, LAT - 4.1 mm, DV - 3.3 mm. For vHF: anterior, AP - 5.28 mm from Bregma, LAT – 4.9 mm, DV - 7.4 mm; posterior, AP – 5.8 mm from Bregma, LAT - 5.2 mm, DV - 7.0 mm. And for cRSC, anterior, AP – 5.8 mm from Bregma, LAT – 0.9 mm, DV - 2.1 mm; posterior, AP - 6.6 mm from Bregma, LAT - 1.1 mm; DV - 1.8 mm.

Histology

Rats were deeply anaesthetised with sodium pentobarbital (125mg/kg) and perfused transcardially with 200 ml of chilled saline followed by 200 ml of 4% paraformaldehyde in 0.1 M phosphate buffer solution (pH 7.4). The brains were then removed and postfixed in 4% paraformaldehyde solution overnight at 4°C. Brains were transferred into a 25% sucrose solution in phosphate buffer saline (PBS) for a minimum of 48 h before continuous 40 µm coronal sections were taken using a sliding microtome with a freezing stage (Thermofisher, Christchurch, NZ). Serial sections were collected sequentially into 24 microtubes in cryoprotectant solution (50% PBS, 25% glycerol, and 25% ethylene glycerol).

Fluorescence: All alternate sections (from the odd-numbered tubes) were mounted on gelatine-subbed slides and dried overnight in the dark. They were submerged in graded ethanol (10 dips in each of 70% ethanol, 95% ethanol, 100% ethanol x2), and then cleared in xylene for 5 min before mounting with antifade medium with DAPI (VectaShield® HardSet™ with DAPI, Vector Laboratories, Auckland, NZ) and a coverslip. After curing at room temperature for 15 minutes, the coverslip edges were sealed with clear nail polish. Once dry, the mounted slides were stored in light-protected boxes at 4°C. These sections were processed for fluorescence to verify the infusion site and to examine for labelling in the thalamus. The infusion site was identified in sections showing the maximum intensity of the tracer, guided by the presence of the infusion needle track.

Cresyl violet: After photos were taken of the fluorescent sections, at the infusion sites and in the thalamus, the same sections were re-stained for cresyl violet, thereby providing anatomical references for the fluorescent photos from the exact same sections. Slides were

gently wiped with acetone to remove the nail polish and soaked in PBS overnight at room temperature to remove the coverslips. Before cresyl violet staining, the sections were processed through graded concentrations of ethanol before hydrating in distilled water (1 min) and immersion in 0.5% cresyl violet solution for 12 min. The sections were then rinsed in distilled water, dehydrated through alcohols and placed in an Acid/Alcohol differentiation bath before 100% ethanol followed by Xylene and mounting with Depex and coverslip before drying overnight.

Photomicrographs

Sections were viewed in the dark on a Leica DM6 B upright fluorescence microscope and images captured using a DFC7000T proclass microscope camera using the LAS X 1 imaging and analysis software (RRID:SCR_013673, Leica Microsystems). First, photos were taken using a HC PL FLUOTAR 2.5x objective (25x overall magnification) to capture the infusion sites. Photos of labelled cells in the thalamus were taken from 12 sections from the alternate series of sections. Photos were taken using three independent channels (red and green for the two tracers; blue for DAPI-stained nuclei) representing cells that were excited under the corresponding filter sets for Alexa Fluor® 594, Alexa Fluor® 488, and DAPI, respectively. An overlay image of the three channels combined was also taken. Photos were initially taken using the 2.5x objective to reveal the general pattern of labelled cells before using HC PL FLUOTAR 5x and then 10x objectives (50x and 100x overall magnification, respectively). When the overlaid image in the thalamus showed cells with overlap labelling of both green and red (merged into orange-yellow colour), additional photos were taken using HC PL FLUOTAR 20x and 40x (overall magnification 200x and 400x, respectively) to reveal the double-labelled cells in more detail. After the same sections were stained with cresyl violet they were photographed with the Tile Scan tool on the LAS X software.

Cell counts

We used a semi-quantitative procedure to assess the number of single-stained and double-stained neurons using photos taken using the 20x objective. They were adapted for contrast adjustment within Image J (Rasband, 2011, NIH, USA). We selected one representative case with well-placed infusions for each target pairing (Fig. 1, lower panels). Cell counts were taken from six representative thalamic sections, evenly spaced at about 160 µm throughout the rostro-caudal extent of the anterior thalamus (ranging from Bregma -1.20 mm to Bregma -2.16 mm). Cresyl-stained sections were used to define boundaries of the thalamic nuclei, guided by the Paxinos and Watson atlas (7th edition, 2014). Our focus was the ATN region, and specifically the AM, which therefore allowed us to record bifurcating neurons in the anterior Re in the same sections. Single-labelled cells were counted from the individual red and green channels (corresponding to the fluorophores Alexa Fluor® 594 and Alexa Fluor® 488, respectively). Double-labelled (i.e. bifurcating) neurons were deemed to be those showing evidence of orange-yellow colour from the overlay image of the red and green channels. Double-labelled neurons were established only when the fluorescent labelling surrounded a DAPI-stained nucleus (blue), which was checked using both x20 and x40 objectives. We were careful to ensure that the bifurcating neurons could be confirmed by carefully matching the exact same cell across the independent photos taken using single red and green channels at the identical location in the section. The percentage of double-labelled cells relative to single-labelled cells for each ATN-terminal field pairing was calculated

within each photo. Note, the photos did not cover the whole area of the ATN within the section under examination, and rely only on raw counts. That is, this procedure examined only the boxed region of the photomicrograph (see Figures) where photos were taken and these were used to provide an estimation across the anterior thalamic region. Cell counts were taken from photos across sections to capture a similar location within that structure at six rostral-caudal levels across different rats. To standardise counts, any cell that straddled the ventral or right edge of the photomicrograph was counted, whereas those across the dorsal or left edge were not counted. Counts were made by a researcher blind to the experimental conditions. Counts were made on a subset of photographs by a second researcher, without knowledge of the original counts, which confirmed good inter-rater reliability ($R^2 = 0.99$, $p < 0.01$).

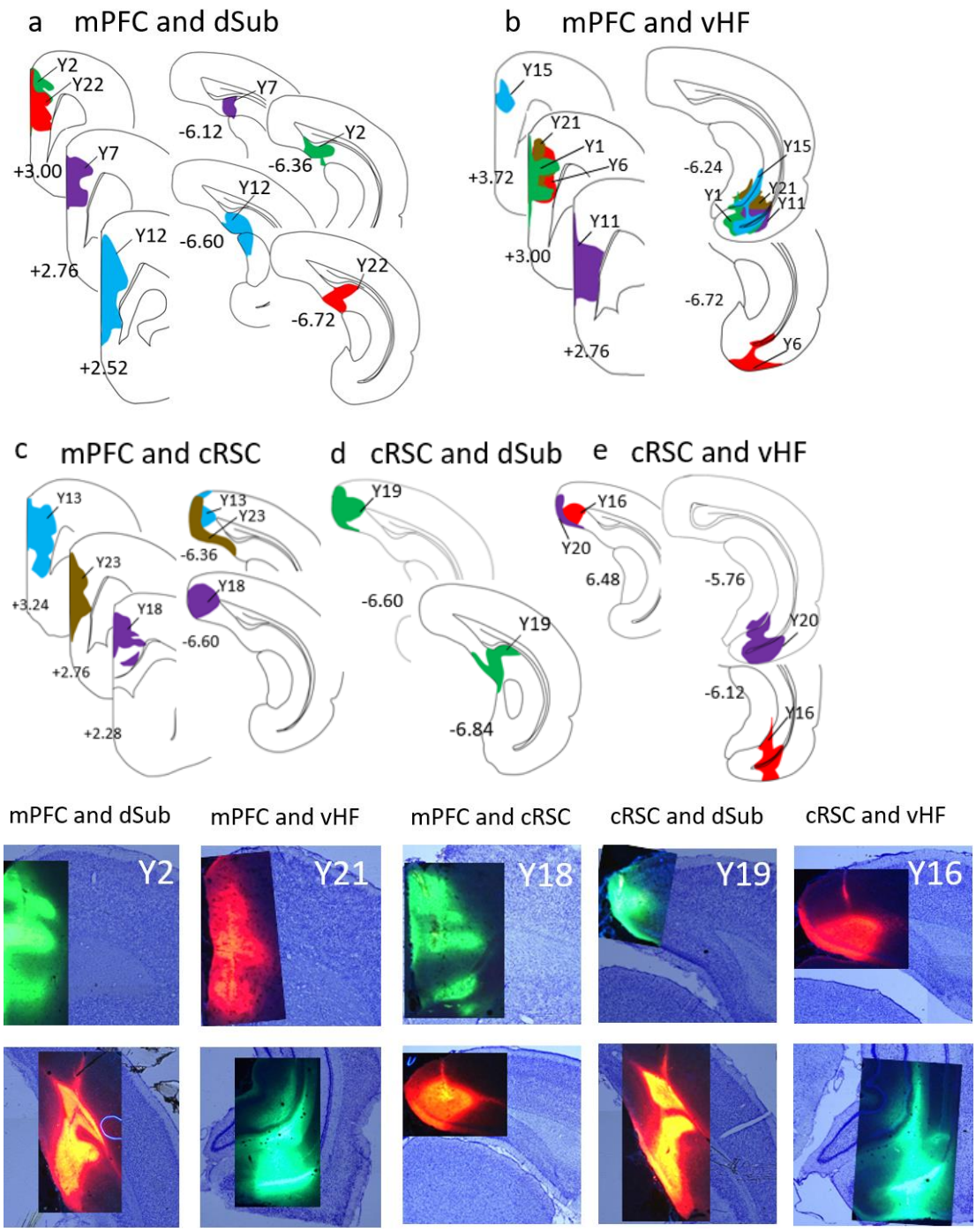

Fig. 1. Upper panels show schematic representations of paired infusions of neurotracers AF CTB 488 and AF CTB 594 for individual rats in the five paired structures used. Within each terminal-field pairing, the same rat is shown using the same colour and different rats are shown with different colours. The lower pair of rows show photomicrographs of the infusions, overlaid on the same section that was counterstained with cresyl violet, for one representative rat per neurotracer pairing. The upper row of this pair shows the infusion in the first of the paired structures and the lower row shows the corresponding infusion in the second terminal field. Note that none of the infusions spread to the contralateral hemisphere. AF CTB: Cholera Toxin Subunit B (Recombinant) Alexa Fluor™; cRSC: caudal retrosplenial cortex; dSub: dorsal subiculum; mPFC: medial prefrontal cortex; vHF: ventral hippocampal formation.

Results

Hemispheric expression of neurotracer labelling

Uptake of the neurotracers in ATN neurons, in all cases, was almost exclusively ipsilateral to the hemisphere in which the infusions were made. In all cases (i.e., after tracer infusions in all the four terminal field structures), labelling was also found in the Re, which rarely crossed the midline. Unlike the ATN and the Re, there was some contralateral uptake in the mediodorsal thalamic nucleus associated with the mPFC infusion and some uptake of neurotracer across the midline region of the paraventricular thalamic nucleus associated with the vHF infusion. In both of these cases, however, the contralateral expression was much weaker than that shown on the ipsilateral side.

Expression of bifurcating neurons in the ATN

Fourteen cases had correctly-placed infusions of the retrograde tracers in both target structures (Fig. 1). Fig. 1 also shows the location of the infusions made in case Y6 (excluded due to misplaced vHF infusion). Evidence from counterbalanced infusions of the specific tracers at the two sites for any given paring of neurotracers showed the same pattern of findings. Double-labelled ATN neurons, predominantly in the AM, were found for each of the five neurotracer location pairings (Table 1). Systematic cell counting focused on the AM region (Fig. 2), which is described in detail below. We did not intend systematic counts across tissue sections for cells in the anteroventral thalamic nucleus (AV) and the anterodorsal thalamic nucleus (AD), but we found evidence of bifurcating neurons in these regions also.

mPFC and dSub

These rats were Y2, Y7, Y12, and Y22 (Fig. 1). The mPFC infusion was centred in the dorsal and mid-ventral aspects of the mPFC, including A32D and A32V in both Y2 and Y22, and A24b and A24a in both Y7 and Y12. Note that A24b and A32D are generally equivalent to the cingulate cortex area 1 (Cg1) and A24a and A32V represent much of what is also known as prelimbic cortex (PrL). There was additional posterior and ventral spread in the mPFC in Y12, at A33 and A25 (i.e., PrL and infralimbic cortex, IL). The dSub infusion included the subiculum in all cases and the postsubiculum in all cases except Y7. Neurotracer was also present in the presubiculum in Y22.

As shown in Table 1, the pattern of labelled cells in the thalamus was consistent across all four rats. The mPFC infusion produced dual-labelled neurons predominantly in the AM, which was most prominent in the lateral and dorsal regions (Fig. 3). There was some dual-labelling in the AV, usually in the ventrolateral part of the AV (AVVL). Single labelling after the dSub infusion was associated with neurons located in all three nuclei (AM, AV and AD), but most strongly in AV and AD regions.

mPFC and vHF

These rats were Y1, Y11, Y15, and Y21 (Fig. 1). The mPFC infusion was centred at A32D and A32V (i.e. Cg1 and PrL) in four cases. The infusion in Y11 was more posterior and ventral, spreading to A24a and A25 (i.e. PrL and IL). The vHF infusion was centred in the ventral subiculum in four cases and included entorhinal cortex in all cases. There was some spread into the molecular layer of the dentate gyrus (MoDG) in cases Y15 and Y21.

Bifurcating cells from infusions in mPFC and in vHF were again almost exclusively found in the AM in all 4 rats. There were some bifurcating neurons in the dorsomedial part of the AV (AVDM) in rat Y15 and some in the interanterodorsal thalamic nucleus (IAD) in rat Y21 (Table 1). Single projecting cells were almost exclusively found in the AM in all four rats. Case Y6, with an infusion in only the entorhinal cortex and not the vHF, also showed some double-labelled cells in the AM.

mPFC and cRSC

These cases were Y13, Y18 and Y23 (Fig. 1). The mPFC infusion was evident in both dorsal and ventral mPFC in Y13, covering A32D, A32V, and A25 (Cg1, PrL, and IL). The mPFC infusion was more posterior in the other two cases, which was in A24b and A24a (Cg1 and cingulate cortex, area 2 [Cg2]) for Y18; and Cg1 and PrL for Y23. In all cases, the cRSC, infusions covered A30, A29c, and A29b (retrosplenial dysgranular cortex [RSD], retrosplenial granular cortex c region [RSGc], and retrosplenial granular cortex b region [RSGb]), with additional spread in A29a (retrosplenial granular cortex a region [RSGa]) in Y23.

Evidence of bifurcating neurons was found in the AM in all three cases. There were bifurcating cells also for the AV in cases 18 and 23. In all three cases, single-projecting cells from the infusions in the mPFC were again located in the AM with less evidence of single-labelled cells in the AV. A few cells labelled by mPFC infusions were scattered in the IAD in Y13 and Y23. Single-labelled cells from the cRSC infusions were clearly evident in the AD and AV regions in all three rats, but there were also single-labelled cells in the AM. In the fourth case, Y3, the cRSC infusion failed and single-labelled cells from the mPFC infusion were found in the AM and IAD.

cRSC and dSub

There was one case (Case Y19), which had a cRSC infusion that included A30, A29c, and A29b (also known as RSD, RSGc, and RSGb) and a dSub infusion that included the subiculum, the postsubiculum, and presubiculum (Fig. 1). Both double-labelled and single-labelled cells were evident across all three ATN subnuclei. Double labelled cells were more frequently found in the AM and in the region where the AVDM intersects with the AD and in the AVVL. The single-labelled cells were more frequent in the AVDM after cRSC infusion, and in the AD, AM and AVVL following dSub infusion. The second case, Y4, only had a successful infusion in the dSub (the cRSC infusion failed in this rat). For Y4, single-labelled cells from the dSub infusion were found in all three ATN subnuclei, similar to the single-labelled cells found for Y19.

cRSC and vHF

These cases were Y16, and Y20 (Fig. 1). The cRSC infusion was located in A29c and A29b (i.e. RSGc and RSGb) for both rats, with some tracer in A29a (i.e. RSGa) for Y20. Both vHF infusions included the ventral subiculum with additional spread into the entorhinal cortex in Y16 and in the MoDG in Y20.

Bifurcating cells were found in the AM and to a lesser extent in the AD in both cases; case Y16 also showed double-labelled cells in the IAD. The cRSC infusion labelled cells in the AM, AV and AD for both cases. The vHF infusion produced labelled cells in the AM and AD

for both cases. Case Y16 showed single-labelled cells from both infusions in the IAD. The third case, Y5, had a failed infusion in the cRSC and showed single labelled cells from the vHF infusion in the AM and IAD.

Cell counts in the ATN

Estimates of the number of single-labelled and double-labelled neurons focused on the AM subregion for the reasons given earlier. The outcomes for a representative rat for each of the five neurotracer pairings are shown in Fig. 2. A photomicrograph example of the bifurcating AM neurons after neurotracer infusions in the mPFC and dSub (Y2) is shown in Fig. 3.

For the mPFC and dSub pairing (Y2), the proportion of bifurcating neurons in the AM was substantial (36% overall) and consistently high throughout this subnucleus (Fig. 2a). This proportion rose from 20% for the most anterior section (at Bregma -1.28 mm) to about 40% for the remainder of the AM except for the most posterior section where it fell to 33% (at Bregma -2.08 mm). The fraction of double labelled cells was slightly higher in the dSub-projecting population than in the mPFC-projecting population (average 61% and 48%, respectively).

For the mPFC and cRSC pairing (Y18, the proportion of bifurcating AM neurons was also high (20% overall). It was 30% for the most anterior AM region with generally lower proportions in photographs from more caudal sections (Fig. 2c). A higher fraction of double-labelled cells was found in the cRSC-projecting cells (47%) compared to that in the mPFC-projecting cells (27%).

The proportion of AM bifurcating cells was much lower for the other three pairings, averaging 6% for mPFC and vHF, 11% for cRSC and dSub, and 11% for cRSC and vHF (Fig. 2). These proportions were generally consistent across the anterior to posterior extent of the AM. In the mPFC and vHF pairing, the double-labelled cells comprised almost half of the total subpopulation of vHF-projecting cells (50%) but far lower for that of the mPFC-projecting cells (7%), which was possibly related to the substantially lower total number of cells that projected to the vHF than projected to the mPFC. For the cRSC and dSub pairing, the fraction of double labelled cells was considerably higher in the cRSC-projecting cells (40%) than in the dSub-projecting cells (13%), perhaps now reflecting a much higher total number of dSub-projecting cells than cRSC-projecting cells. With respect to the cRSC and vHF pairing, the fraction of double-labelled cells was considerably higher in the vHF-projecting cells (43%) than in the cRSC-projecting cells (13%), which may be associated with the disproportionally higher total number of cRSC-projecting cells than vHF-projecting cells that was captured by the infusions made.

We have only a preliminary analysis of the AV and AD, as a systematic series of photographs was not taken for these nuclei. Double-labelled cells were found in the AV for all neurotracer pairings except for the cRSC and vHF pairing. Double-labelled cells were found in the AD in the cRSC and dSUB pairing and the cRSC and vHF pairing. Doublelabelling in these regions appeared to be generally less consistent across the anterior-posterior extent of the ATN than was found for the AM. For the cRSC and dSUB pairing, however, inspection of available photomicrographs for Y19 suggested more consistent double labelling across the rostral-caudal extent of the ATN in this instance. Where

photomicrographs were available, cell counts for AV suggested ~8-20% double-labelled cells for the mPFC and dSUB pairing, 23% for the mPFC and vHF pairing, 24-37% for the mPFC and cRSC pairing, and 9-22% for the cRSC and dSUB pairing. Cell counts for AD suggested 8-31% of double-labelled cells for the cRSC and dSUB pairing, and 11% for the cRSC and vHF pairing.

Bifurcating neurons in the Re

In the same sections that were assessed for ATN cell labelling, single-labelled cells in the Re, and the adjacent ventral Re, were found after neurotracer infusions placed in all four terminal sites. Double-labelled cells in the Re were evident in all five neurotracer pairings (Fig. 4). As with the ATN, the largest proportion of double-labelled cells was found with the mPFC and dSub pairing in case Y2, which averaged 31% and was generally consistent throughout the Re to the extent that we examined sections showing the ATN. There was also a relatively high proportion of bifurcating cells in the Re associated with the mPFC and cRSC pairing (26%) in rat Y18. We did not record all the intended anterior to posterior photographs for the Re in the other three infusion pairings (mPFC and vHF; cRSC and dSub; cRSC and vHF), but the available evidence in Fig. 4 suggests perhaps more bifurcating Re neurons for the pairing mPFC with vHF (11%) than was found for the AM for this pairing (6%), but a similar proportion of bifurcating neurons for cRSC with dSub (12%) and for cRSC with vHF (14%) in Re as was found for AM (11% in both cases).

In the Re, the mPFC and dSub pairing, the mPFC and vHF pairing, and the cRSC and vHF pairing all produced similar fraction of double-labelled cells relative to the total population that projected to each of the former and latter sites within each pair of infusions (45% and 52%, for mPFC and dSub, respectively; 19% and 24% to mPFC and vHF, respectively; 25% and 27% for cRSC and vHF, respectively).

For the mPFC and cRSC pairing, however, the proportion of double labelled cells in the Re was considerably higher in the cRSC-projecting population (61%), being almost double that of the mPFC-projecting population (32%). Similarly, for the cRSC and dSub pairing, the double-labelled cells comprised a significantly higher proportion of the cRSC-projecting population (50%) compared to the dSub-projecting population of cells (13.2%) in the Re, possibly due to the much higher total number of cells labelled by the dSub infusion than by the cRSC infusion.

Bifurcating neurons in other adjacent nuclei

The mPFC and dSUB infusion pairing and the mPFC and vHF infusion pairing produced a few double labelled cells in the mediodorsal thalamic nucleus (MD), paratenial thalamic nucleus, ventral anterior thalamic nucleus, ventromedial thalamic nucleus, and Rhomboid nucleus (Rh). Some double-labelled cells were found in the MD in the group given the mPFC and cRSC pairing. In addition, the cRSC and vHF infusions produced some double-labelled cells in the Rh. Casual observation suggested that the number of these cells was low in these nuclei. Single labelled cells were prominent in these adjacent regions mentioned above. In addition, cRSC, dSub, and vHF infusions also produced single labelling in the laterodorsal thalamic nucleus, but we did not see any evidence of bifurcating cells.

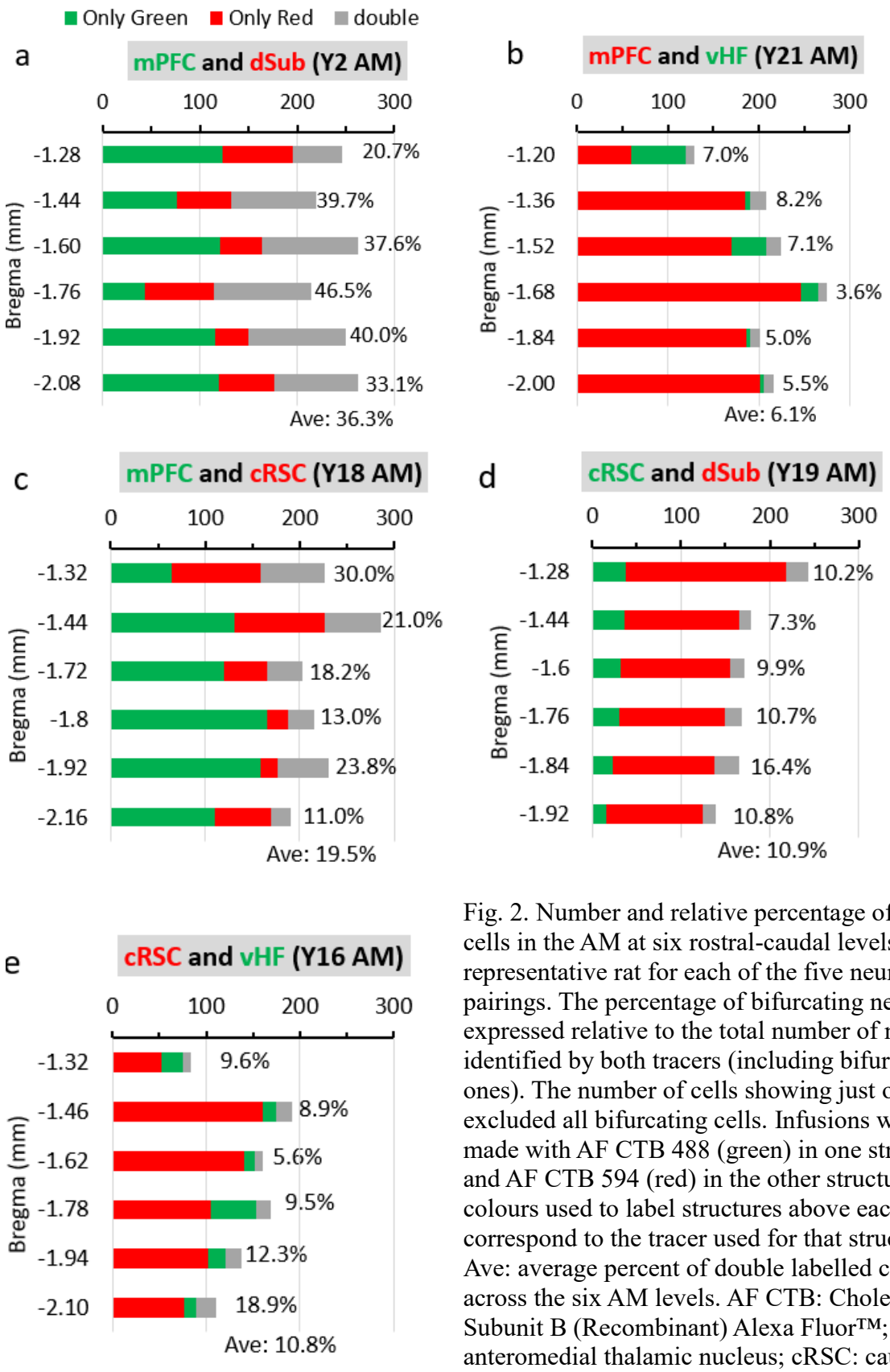

Fig. 2. Number and relative percentage of labelled cells in the AM at six rostral-caudal levels in a representative rat for each of the five neurotracer pairings. The percentage of bifurcating neurons is expressed relative to the total number of neurons identified by both tracers (including bifurcating ones). The number of cells showing just one label excluded all bifurcating cells. Infusions were made with AF CTB 488 (green) in one structure and AF CTB 594 (red) in the other structure. The colours used to label structures above each panel correspond to the tracer used for that structure. Ave: average percent of double labelled cells across the six AM levels. AF CTB: Cholera Toxin Subunit B (Recombinant) Alexa Fluor™; AM: anteromedial thalamic nucleus; cRSC: caudal retrosplenial cortex; dSub: dorsal subiculum; mPFC: medial prefrontal cortex; vHF: ventral hippocampal formation.

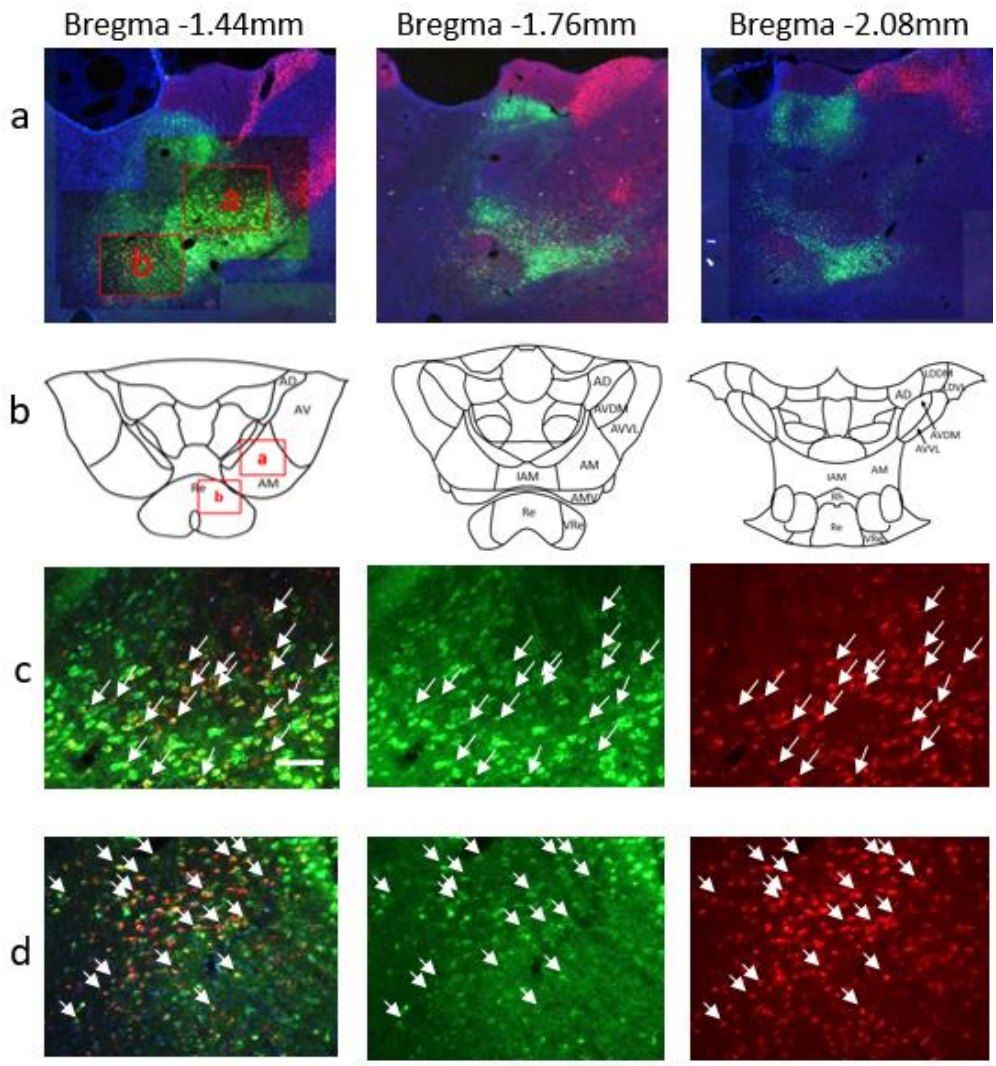

Fig. 3. Single and double labelled cells in the AM and Re at three rostral-caudal levels in Y2 after infusion of AF CTB 488 (green) into mPFC and AF CTB 594 (red) into dSub. The position of the red-box insets in the first panel of row (a) are depicted on the atlas outline in row (b) at Bregma -1.44 mm. (c) Higher magnification view of inset box a within the top left panel, showing the AM, with examples of double-labelled cells indicated by white arrows in the left panel and corresponding green and red labelled cells in the middle and right panels. Row (d) shows the corresponding fluorescence but now in the inset box b from row (a), which is the Re region. Scale bar 100um in c. AD: anterodorsal thalamic nucleus; AF CTB: Cholera Toxin Subunit B (Recombinant) Alexa Fluor™; AM: anteromedial thalamic nucleus; AMV: anteromedial thalamic nucleus, ventral part; AV: anteroventral thalamic nucleus; AVDM: dorsomedial part of the AV; AVVL: ventrolateral part of the AV; IAM: interanteromedial thalamic nucleus; LDDM: laterodorsal thalamic nucleus, dorsomedial part; LDVL: laterodorsal thalamic nucleus, ventrolateral part; Re: reuniens thalamic nucleus; Rh: rhomboid thalamic nucleus; vRe: ventral reuniens thalamic nucleus.

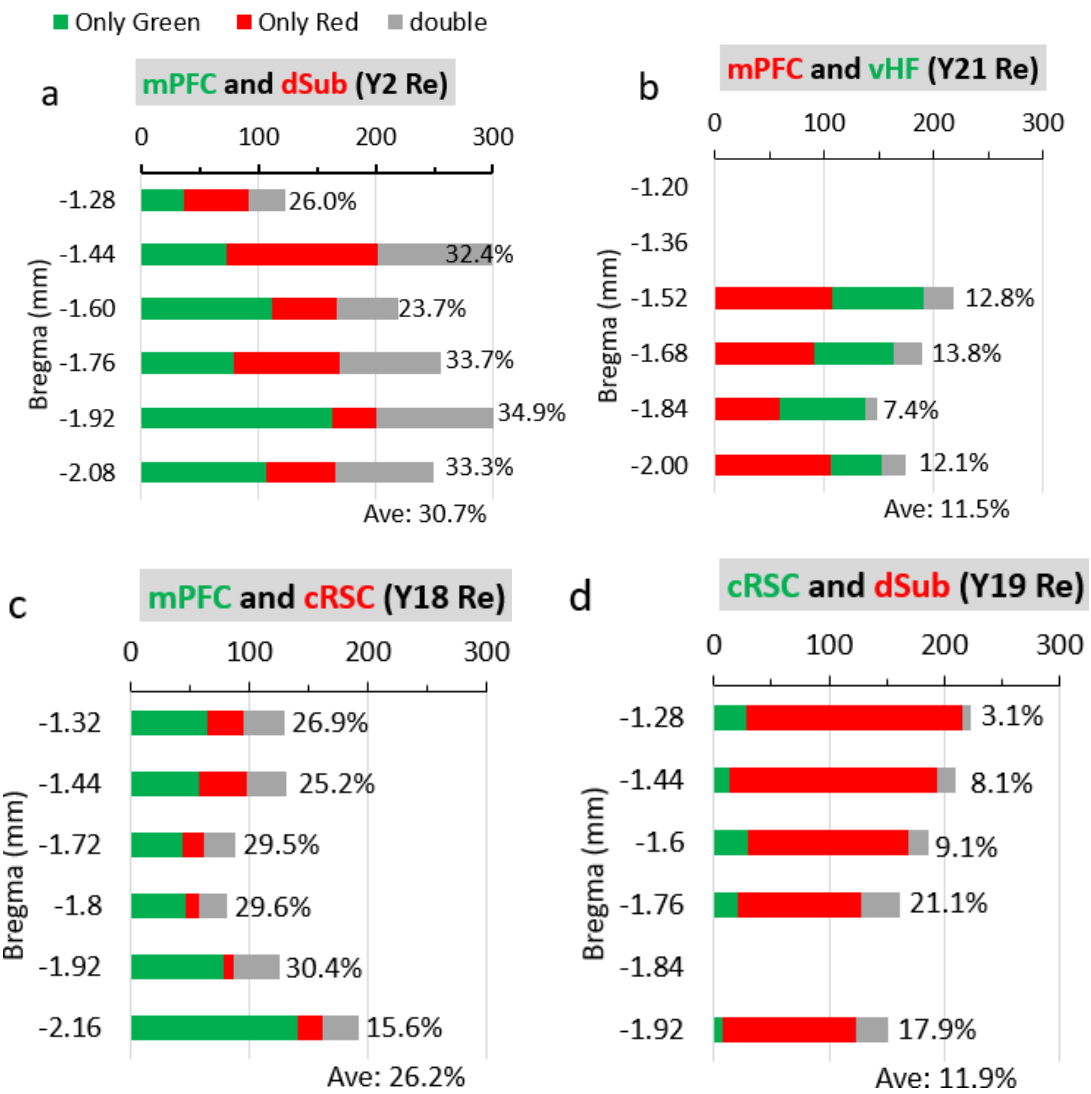

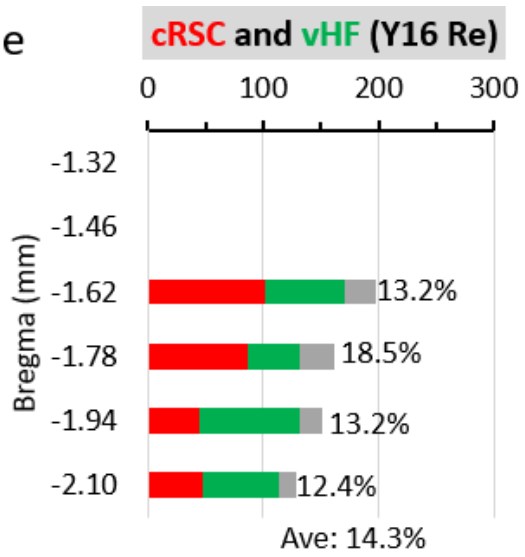

Fig. 4. Number and relative percentage of labelled cells in the Re across rostral-caudal levels in a representative rat for each of the five neurotracer pairings. The percentage of bifurcating neurons is expressed relative to the total number of neurons identified by both tracers (including bifurcating ones). The number of cells showing just one label excluded all bifurcating cells. Infusions were made with CTB 488 (green) in one structure and CTB 594 (red) in the other structure. The colours used to label structures above each panel correspond to the tracer used for that structure. Photos were not taken at levels where no bar is shown. Ave: average percent of double labelled cells across all the available levels of Re for that rat; AF CTB: Cholera Toxin Subunit B (Recombinant) Alexa Fluor™; cRSC: caudal retrosplenial cortex; dSub: dorsal subiculum; mPFC: medial prefrontal cortex; Re: reuniens thalamic nucleus; vHF: ventral hippocampal formation.

Discussion

We used a double retrograde CTB fluorescent tracing technique to examine the potential for bifurcating ATN neurons projecting to separate, distantly-located cortical regions. Based on single labelling, we replicated previous evidence that the ATN represent a key node within an extended memory system, with multiple efferents that can exert an influence on the mPFC, the RSC and the HF (Bubb et al., 2017; Shibata, 1993b, 1993a; van Groen et al., 1999; van Groen and Wyss, 1995). We now show, however, that an abundant number of bifurcating neurons are found in the lateral and dorsal part of the AM subnucleus. Previously, bifurcating ATN neurons were reported by one study that only examined the cingulate gyrus; only AM neurons showing collateralization for the most distally-located regions of this limbic cortex (Horikawa et al., 1988). Here we examined the existence of such neurons by considering much wider brain circuits encompassing a broad range of cortical and hippocampal structures. The strength and potential impact of this new evidence was reinforced by finding bifurcating neurons for all five of the neurotracer pairings examined, specifically mPFC and dSub, mPFC and vHF, mPFC and cRSC, cRSC and dSub, and cRSC and vHF. Like previous descriptions based on single ATN efferents (Mathiasen et al., 2017), the bifurcating ATN efferents that we observed here were also exclusively unilateral. Although not examined in the same detail, bifurcating neurons were also found in the AV and AD subnuclei of the ATN. Previously bifurcating AV and AD neurons were described for the posterior regions of the cingulate cortex (Horikawa et al., 1988).

The classic view of the ATN's role in a hippocampal-diencephalic-cingulate memory network emphasises distinct neural circuits that broadly distinguish the AM, AV and AD subnuclei and their connections (Aggleton et al., 2010; Jankowski et al., 2013; Nelson, 2021; Wright et al., 2013). This perspective is predicated on a system of non-bifurcating ATN efferents that project, separately, to other neocortical and limbic cortex structures. While each thalamic subnucleus exhibits different output mappings, our evidence suggests that some of these distinctions may be less prominent than previously envisaged. Indeed, the relative abundance of bifurcating neurons in the AM, with collaterals to most of the different terminal regions in the extended memory system, has not been anticipated by prior models. This suggests that the AM in particular has more significance for the integration of memory processes than previously recognised.

The proportion of double-labelled cells in the AM region varied across the different terminal structures used for the pairs of neurotracer infusions. The highest proportion (36%; range 21 – 47% across sections) was found after infusions in the mPFC and dSub regions. It should be noted that we did not look systematically across the whole of the AM region, so the true proportion may vary once additional follow-up studies are completed. Nonetheless, comparisons across the different pairings suggested far lower proportions of bifurcating AM neurons (6-11%) after the pairings of mPFC and vHF, cRSC and dSub, and cRSC and vHF. An intermediate level of bifurcating AM neurons was found after neurotracer infusions in the mPFC and cRSC (20%). The proportion of double-labelled cells relative to the corresponding single-labelled cells also varied. In some instances, this proportion was higher for the dSub-projecting neurons (dSub versus mPFC pairing) or lower for the dSub-projecting neurons (dSub versus cRSC). For the vHF-projecting neurons, the proportion of double-labelled cells relative to the single labelled projections was higher than was the case for the corresponding mPFC and cRSC projections. Of course, infusions only spread to a restricted portion of the

relevant target structure and we did not make a systematic comparison across each terminal region; the proportions may vary with the topography of a region and its proximity to other structures. Nonetheless, our findings suggest a different magnitude of influence by bifurcating neurons across the different target structures examined. Estimates derived from infusions across a wider area of the subiculum would reinforce the full extent of collaterals from ATN neurons, and specifically AM neurons, on this important hippocampal structure. It would be interesting to examine additional regions, especially more caudal aspects of the ACC and the more rostral aspects of the RSC. We have only looked at bifurcations for pairs of ATN efferent targets. It is possible that some neurons have a yet more widespread influence by projecting to more than two target structures.

Although our focus was the AM subregion of the ATN, we also examined bifurcating neurons in the adjacent Re. That is, we are able to comment on those parts of the Re that are located ventral and medial to the AM. With respect to mPFC and vHF neurotracer pairing, our data were consistent with similar work on the Re (Hoover and Vertes, 2012; Varela et al., 2014), which increases confidence in our overall findings. Like these previous studies, this neurotracer pairing produced a modest proportion of bifurcating Re cells throughout the region examined. In our case, the proportion was a little higher for the pairing of mPFC and vHF (11.5%), because previous work reported about 3-9% of labelled bifurcating cells, although the average was greater (8%) when CTB tracers were used (Varela et al., 2014). The previous Re studies have focused on the mPFC paired with the vHF, but they used a small volume of neurotracer infusions whereas we used relatively large volumes of neurotracers, and in two sites per target, to ensure that we did not underestimate the presence of bifurcating neurons. Another difference was that prior work on the Re explicitly targeted the mPFC and ventral hippocampal CA1 region, which produced a larger number of bifurcating Re neurons compared to dorsal CA1 infusions, but there tended to be more labelling when the infusions included the ventral subiculum. By contrast, our infusions were explicitly aimed at the ventral subiculum and included the entorhinal region. There is no evidence that the ATN project to the dorsal CA1 (Bubb et al., 2017; Mathiasen et al., 2020; Nelson, 2021), so we did not focus our infusions on the CA1 region. We note that one study found evidence that the ventral regions of the AM project to the ventral CA1 in addition to the subiculum (de Lima et al., 2017). Beyond this previous work of bifurcating neurons in the Re, however, we found new evidence that Re neurons send collaterals to several other regions, including mPFC and dSub, mPFC and cRSC, cRSC and dSub, and cRSC and vHF. Moreover, the proportion of bifurcating Re neurons is two or three-fold for the mPFC pairing with dSub and cRSC than was the case even for mPFC and vHF. While these proportions must be treated with caution, given our methodology, they demonstrate a much wider influence of bifurcating Re neurons on the extended hippocampal memory system than previously described. Other studies have found that the Re send collaterals to both mPFC and other (non-medial temporal lobe) regions such as the nucleus accumbens (see Cassel et al., 2013). It is possible, then, that a wider range of target structures that receive collaterals needs also to be examined with respect to the AM region.

Naturally, the specific functional influence of the bifurcating Re neurons has been emphasised (Hoover and Vertes, 2012; Varela et al., 2014). A reasonable assumption is that they facilitate direct coordination between PFC and hippocampal regions to enhance interactions between these two key memory regions in the brain (Eichenbaum, 2017). We

can, therefore, posit a similar role in facilitating interactions among key memory structures for the more numerous bifurcating AM neurons, especially the high number of cells sending collaterals to both mPFC and dSub. Both the ATN and the Re have been associated with learning and memory processes, but there is sound evidence to consider their roles as different (Mathiasen et al., 2020). There is substantial evidence for the ATN's role in supporting episodic-like memory, in particular, although most of this evidence concerns spatial memory and navigation (Aggleton and Nelson, 2015; Nelson, 2021). By contrast, the influence of the Re may be more relevant for selecting from competing memories and long-term memory consolidation (de Vasconcelos and Cassel, 2015; Ferraris et al., 2021). It remains to be seen whether the bifurcating subset of neurons in the AM and the Re share similar properties. Nonetheless, the literature supporting a critical role for the ATN in memory continues to gain momentum and the discovery of bifurcating neurons in the ATN may help answer why injury in or dysfunction of this region is strongly associated with diencephalic amnesia and other disorders associated with poor memory (Aggleton et al., 2016; Carlesimo et al., 2011; Perry et al., 2019). Electrophysiological recordings in drug-resistant epilepsy patients suggest that the ATN integrate information from diverse cortical sources during encoding to guide successful recall (Sweeney-Reed et al., 2021). More recent studies have shown that working memory in both humans and rats can be improved by stimulation of the ATN (Barnett et al., 2021; Liu et al., 2021).

There are some limitations to our study. We detailed evidence on collateral neurons in the AM. As we also found evidence that the AD and AV regions also possess bifurcating neurons that send collaterals to distally-located memory structures, more systematic work focused on these subregions is also warranted. Our analysis on the AM was only semi-quantitative, albeit similar to previous work on the Re. Unbiased stereology is needed to better define the quantitative evidence reported here. As is common in neuroanatomical tracer studies, relatively few animals were used in each group, especially pairings that did not include the mPFC. Nonetheless, the results were consistent across rats. More pairings across and within the many different terminal fields of ATN efferents require evaluation in the future. It would also be valuable to know whether the same or different terminal neurons send reciprocal ATN afferents. The areal and laminar distribution of the axonal collaterals, and the electrophysiological properties of the bifurcating neurons relative to the non-bifurcating neurons, may provide mechanistic insights to the functional properties of this important thalamic region.

The discovery of numerous bifurcating neurons in the ATN suggests the need for a conceptual realignment of the ATN, away from a focus on segregated neural circuits, and more explicitly towards concepts of control and integration of memory information across the extended memory system (Wolff and Vann, 2019). Future work can now reveal the specific functional roles of the bifurcating ATN (and Re) neurons in support of memory. We suggest that these ATN neurons in particular play a role in the explicit binding of two or more elements associated with a memory episode. To learn if we are correct will demand non-conventional memory tests that go beyond the classic evidence of the ATN's role in allocentric learning and navigation (Aggleton and Nelson, 2015; Dalrymple-Alford et al., 2015; Hamilton and Dalrymple-Alford, 2021; Mathiasen et al., 2020; Nelson, 2021; Wolff et al., 2006).

References

Aggleton JP. 2008. EPS Mid-Career Award 2006. Understanding anterograde amnesia: disconnections and hidden lesions. *Q J Exp Psychol (Hove)*. doi:10.1080/17470210802215335

Aggleton JP, Nelson AJD. 2015. Why do lesions in the rodent anterior thalamic nuclei cause such severe spatial deficits? *Neurosci Biobehav Rev*. doi:10.1016/j.neubiorev.2014.08.013

Aggleton JP, O'Mara SM, Vann SD, Wright NF, Tsanov M, Erichsen JT. 2010. Hippocampal-anterior thalamic pathways for memory: Uncovering a network of direct and indirect actions. *Eur J Neurosci*. doi:10.1111/j.1460-9568.2010.07251.x

Aggleton JP, Pralus A, Nelson AJD, Hornberger M. 2016. Thalamic pathology and memory loss in early Alzheimer's disease: Moving the focus from the medial temporal lobe to Papez circuit. *Brain*. doi:10.1093/brain/aww083

Barnett SC., McNaughton N., Perry BAL., Young CK., Hughes SM., Parr-Brownlie LC. and Dalrymple-Alford J. (2021) Anterior thalamic nuclei neurons sustain memory.

Bubb EJ, Kinnavane L, Aggleton JP. 2017. Hippocampal–diencephalic–cingulate networks for memory and emotion: An anatomical guide. *Brain Neurosci Adv* **1**:239821281772344. doi:10.1177/2398212817723443

Carlesimo, G. A., Lombardi, M. G., Caltagirone, C., 2011. Vascular thalamic amnesia: a reappraisal. Neuropsychologia, 49(5), 777-789.

Cassel JC, De Vasconcelos AP, Loureiro M, Cholvin T, Dalrymple-Alford JC, Vertes RP. The reuniens and rhomboid nuclei: neuroanatomy, electrophysiological characteristics and behavioral implications. Progress in neurobiology. 2013 Dec 1;111:34-52.

Conte WL, Kamishina H, Reep RL. 2009a. The efficacy of the fluorescent conjugates of cholera toxin subunit B for multiple retrograde tract tracing in the central nervous system. *Brain Struct Funct* **213**:367–373. doi:10.1007/s00429-009-0212-x

Conte WL, Kamishina H, Reep RL. 2009b. Multiple neuroanatomical tract-tracing using fluorescent Alexa Fluor conjugates of cholera toxin subunit B in rats. *Nat Protoc* **4**:1157–1166. doi:10.1038/nprot.2009.93

Dalrymple-Alford JC, Harland B, Loukavenko EA, Perry B, Mercer S, Collings DA, Ulrich K, Abraham WC, McNaughton N, Wolff M. 2015. Anterior thalamic nuclei lesions and recovery of function: Relevance to cognitive thalamus. *Neurosci Biobehav Rev*. doi:10.1016/j.neubiorev.2014.12.007

de Lima MAX, Baldo MVC, Canteras NS. 2017. A role for the anteromedial thalamic nucleus in the acquisition of contextual fear memory to predatory threats. *Brain Struct Funct* **222**:113–129. doi:10.1007/s00429-016-1204-2

de Vasconcelos AP, Cassel J-C. 2015. The nonspecific thalamus: A place in a wedding bed for making memories last? *Neurosci Biobehav Rev*. doi:10.1016/j.neubiorev.2014.10.021

Eichenbaum H. 2017. Prefrontal-hippocampal interactions in episodic memory. *Nat Rev Neurosci*. doi:10.1038/nrn.2017.74

Ferraris M, Cassel JC, Pereira de Vasconcelos A, Stephan A, Quilichini PP. 2021. The nucleus reuniens, a thalamic relay for cortico-hippocampal interaction in recent and remote memory consolidation. *Neurosci Biobehav Rev* **125**:339–354. doi:10.1016/J.NEUBIOREV.2021.02.025

Hamilton JJ. and Dalrymple-Alford J. (2021) Anterior thalamic nuclei: A critical substrate for non-spatial paired-associate memory. bioRxiv BIORXIV/2021/456360 http://dx.doi.org/10.1101/2021.08.14.456360.

Harding A, Halliday G, Caine D, Kril J. 2000. Degeneration of anterior thalamic nuclei differentiates alcoholics with amnesia. *Brain* **123**:141–154. doi:10.1093/brain/123.1.141

Hoover WB, Vertes RP. 2012. Collateral projections from nucleus reuniens of thalamus to hippocampus and medial prefrontal cortex in the rat: A single and double retrograde fluorescent labeling study. *Brain Struct Funct* **217**. doi:10.1007/s00429-011-0345-6

Horikawa K, Kinjo N, Stanley LC, Powell EW. 1988a. Topographic organization and collateralization of the projections of the anterior and laterodorsal thalamic nuclei to cingulate areas 24 and 29 in the rat. *Neurosci Res* **6**:31–44. doi:10.1016/0168-0102(88)90004-1

Jankowski MM, Ronnqvist KC, Tsanov M, Vann SD, Wright NF, Erichsen JT, Aggleton JP, O'Mara SM. 2013. The anterior thalamus provides a subcortical circuit supporting memory and spatial navigation. *Front Syst Neurosci* **7**:45. doi:10.3389/fnsys.2013.00045

Kim E, Ku J, Namkoong K, Lee W, Lee KS, Park JY, Lee SY, Kim JJ, Kim SI, Jung YC. 2009. Mammillothalamic functional connectivity and memory function in Wernicke's encephalopathy. *Brain* **132**:369–376. doi:10.1093/brain/awn311

Kopelman MD. 2015. What does a comparison of the alcoholic Korsakoff syndrome and thalamic infarction tell us about thalamic amnesia? *Neurosci Biobehav Rev*. doi:10.1016/j.neubiorev.2014.08.014

Liu J, Yu T, Wu J, Pan Y, Tan Z, Liu R, Wang X, Ren L, Wang L, 2021. Anterior thalamic stimulation improves working memory precision judgments, Brain Stimulation, doi: https://doi.org/10.1016/j.brs.2021.07.006.

Maillard A, Laniepce A, Cabé N, Boudehent C, Chételat G, Urso L, Eustache F, Vabret F, Segobin S, Pitel A-L. 2021. Temporal Cognitive and Brain Changes in Korsakoff Syndrome. *Neurology* **96**:e1987–e1998. doi:10.1212/wnl.0000000000011749

Mathiasen ML, Dillingham CM, Kinnavane L, Powell AL, Aggleton JP. 2017. Asymmetric cross-hemispheric connections link the rat anterior thalamic nuclei with the cortex and hippocampal formation. *Neuroscience* **349**:128. doi:10.1016/j.neuroscience.2017.02.026

Mathiasen ML, O'Mara SM, Aggleton JP. 2020. The anterior thalamic nuclei and nucleus reuniens: So similar but so different. *Neurosci Biobehav Rev*. doi:10.1016/j.neubiorev.2020.10.006

Nelson AJD. 2021. The anterior thalamic nuclei and cognition: A role beyond space? *Neurosci Biobehav Rev*. doi:10.1016/j.neubiorev.2021.02.047

Perry JC, Pakkenberg B, Vann SD. 2019. Striking reduction in neurons and glial cells in anterior thalamic nuclei of older patients with Down syndrome. *Neurobiology of aging*. **75**:54-61. doi.org/10.1016/j.neurobiolaging.2018.11.009

Rasband, W.S., ImageJ. 2011. U. S. National Institutes of Health, Bethesda, Maryland, USA, https://imagej.nih.gov/ij/, 1997-2018.

Shibata H. 1993a. Efferent projections from the anterior thalamic nuclei to the cingulate cortex in the rat. *J Comp Neurol* **330**:533–542. doi:10.1002/cne.903300409

Shibata H. 1993b. Direct projections from the anterior thalamic nuclei to the retrohippocampal region in the rat. *J Comp Neurol* **337**:431–445. doi:10.1002/cne.903370307

Sripanidkulchai K, Wyss JM. 1986. Thalamic projections to retrosplenial cortex in the rat. *J Comp Neurol* **254**:143–165. doi:10.1002/cne.902540202

Sweeney-Reed CM, Buentjen L, Voges J, Schmitt FC, Zaehle T, Kam JWY, Kaufmann J, Heinze HJ, Hinrichs H, Knight RT, Rugg MD. 2021. The role of the anterior nuclei of the thalamus in human memory processing. *Neurosci Biobehav Rev*. doi:10.1016/j.neubiorev.2021.02.046

van Groen T, Kadish I, Wyss JM. 1999. Efferent connections of the anteromedial nucleus of the thalamus of the rat. *Brain Res Rev*. doi:10.1016/S0165-0173(99)00006-5

van Groen T, Michael Wyss J. 1990. Connections of the retrosplenial granular a cortex in the rat. *J Comp Neurol* **300**:593–606. doi:10.1002/cne.903000412

van Groen T, Wyss JM. 1995. Projections from the anterodorsal and anteroveniral nucleus of the thalamus to the limbic cortex in the rat. *J Comp Neurol* **358**:584–604. doi:10.1002/cne.903580411

Vann SD, Aggleton JP, Maguire EA. 2009. What does the retrosplenial cortex do? *Nat Rev Neurosci*. doi:10.1038/nrn2733

Varela C, Kumar S, Yang JY, Wilson MA. 2014. Anatomical substrates for direct interactions between hippocampus, medial prefrontal cortex, and the thalamic nucleus reuniens. *Brain Struct Funct* **219**. doi:10.1007/s00429-013-0543-5

Wolff M, Alcaraz F, Marchand AR, Coutureau E. 2015. Functional heterogeneity of the limbic thalamus: From hippocampal to cortical functions. *Neurosci Biobehav Rev*. doi:10.1016/j.neubiorev.2014.11.011

Wolff M, Gibb SJ, Dalrymple-Alford JC. 2006. Beyond spatial memory: The anterior thalamus and memory for the temporal order of a sequence of odor cues. *J Neurosci* **26**:2907–2913. doi:10.1523/JNEUROSCI.5481-05.2006

Wolff M, Vann SD. 2019. The cognitive thalamus as a gateway to mental representations. *J Neurosci* **39**:3–14. doi:10.1523/JNEUROSCI.0479-18.2018

Wright NF, Vann SD, Erichsen JT, O'Mara SM, Aggleton JP. 2013. Segregation of parallel inputs to the anteromedial and anteroventral thalamic nuclei of the rat. *J Comp Neurol* **521**:2966–2986. doi:10.1002/cne.23325

Declaration: None of the authors have any competing interests. They acknowledge funding support from the Canterbury Medical Research Foundation, the Neurological Foundation of New Zealand, and the School of Psychology, Speech and Hearing, University of Canterbury, Christchurch, New Zealand.

Table 1. Areas in the ATN that show single and double-labelled cells for each rat after infusion of the retrograde tracers (AF CTB 488 and AF CTB 594) into a pair of structures for five different pairings.

Infusion Pairing	Case	Single label in first structure	Single label in second structure	Double labelling
mPFC and dSub	Y2 (g/r)	AM, IAD, AV(VL)	AM, AD, AV	AM, AV
	Y7 (r/g)	AM, AV(VL)	AM, AD, AV	AM, AV(VL)
	Y12 (r/g)	AM, IAD, AV(VL)	AM, AD, AV	AM, AV(VL)
	Y22 (r/g)	AM, IAD, AV	AM, AD, AV	AM, AV
mPFC and vHF	Y1 (r/g)	AM, IAD	AM	AM
	Y11 (r/g)	AM	AM	AM
	Y15 (g/r)	AM, AV(DM)	AM, AV(DM)	AM, AV(DM)
	Y21 (r/g)	AM, IAD	AM, IAD	AM, IAD
	Y6* (g/r)	AM	AM, AD	AM
mPFC and cRSC	Y13 (r/g)	AM, IAD	AM, AD, AV	AM
	Y18 (g/r)	AM, AV(VL)	AM, AD, AV	AM, AV(VL)
	Y23 (r/g)	AM, IAD, AV	AM, AD, AV	AM, AV
	Y3* (r/g)	AM, IAD	N/A	N/A
cRSC and dSub	Y19 (g/r)	AM, AD, AV	AM, AD, AV(VL)	AM, AD, AV(VL)
	Y4* (r/g)	N/A	AM, AD, AV(VL)	N/A
cRSC and vHF	Y16 (r/g)	AM, AD, IAD, AV	AM, AD, IAD	AM, AD, IAD
	Y20 (g/r)	AM, AD, AV	AM, AD	AM, AD
	Y5* (r/g)	N/A	AM, IAD	N/A

"g" (AF CTB 488) and "r" (AF CTB 594) indicate the tracer colour (green and red) that was infused into the first and the second structure, respectively, for each pairing shown. AD: anterodorsal thalamic nucleus; AM: anteromedial thalamic nucleus; AV: anteroventral thalamic nucleus; AVDM: dorsomedial part of the AV; AVVL: ventrolateral part of the AV; cRSC: caudal retrosplenial cortex; dSub: dorsal subiculum; IAD: interanterodorsal thalamic nucleus; mPFC: medial prefrontal cortex; vHF: ventral hippocampal formation. * = entorhinal but not vHF (Y6) or only one neurotracer was evident (indicated).